Species-specific characterisation of thiolate - disulfide transitions; the influence of molecular structure on disulfide bridge formation and kinetics

PhD thesis

Zoltán Faragó PharmD.

Doctoral School of Pharmaceutical Sciences

Semmelweis University

Supervisor:	Béla Noszál PharmD, DSc
Advisor:	Arash Mirzahosseini PharmD, PhD
Official reviewers:	Gergely Agócs PharmD, PhD
	Tamás Jakusch, PhD

Head of the Complex Examination Committee:

Romána Zelkó PharmD, DSc

Members of the Complex Examination Committee:

Pál Perjési PharmD, CSc

Krisztina Ludányi, PhD

Budapest
2022

Table of contents

List of Abbreviations

Abbreviation	Explanation
ROS	Reactive oxygen species
GSH	Glutathione, in –SH, sulfhydryl form
GSSG	Glutathione, in –S-S-, disulfide form
CSH	Cysteamine
CSSC	Cystamine
MSH	Mercaptoethanol
MSSM	Mercaptoethanol-disulfide
MSSC	Mercaptoethanol-cysteamine heterodisulfide
NMR	Nuclear magnetic resonance
COSY	Correlation spectroscopy
TOCSY	Total correlation spectroscopy
CD	Circular dichroism

1. Introduction

1.1. The Janus-faced reactive oxygen species

Life, as we know it today exists only on Earth and oxygen is an indispensable element of it. (Bucci, 2009)

As a part of cellular metabolism, reactive oxygen species (ROS) are normally produced by biological systems during cellular respiration. At low or moderate levels, ROS exert their beneficial effects on redox homeostasis. These species play a key role in cell proliferation signalling, enhance immunologic defence, support physiological functions, lower the risk of various diseases, including cancer. (Valko et al., 2006, Chatterjee et al., 2007.). ROS activate the p38 signalling pathway resulting in non-apoptotic outcomes, such as differentiation (Choi et al., 2011).

Excessive levels of ROS shift the balance between oxidants and antioxidants in favour of oxidants, generating oxidative stress and causing oxidative damage in cells. Increased level of oxidative stress takes major part in formation and progression of cancer (James E Klaunig, 2018), Alzheimer's disease (D Allan Butterfield, Debra Boyd-Kimball, 2018.), sporadic amyotrophic lateral sclerosis (Emanuele D'Amico, et al., 2013), Parkinson's disease (Grace F Crotty, et al., 2017). Even in some cases of type 2 diabetes, the cause of the disease is elevated oxidative stress (Paria Azimi et al., 2014).

Considering these harmful effects of ROS and oxidative stress, it would be advantageous to have an active pharmaceutical agent to recover this shifted balance between oxidants and antioxidants, to minimise the risk of these diseases.

1.2. Protector against ROS - cysteine

Thiol functional group containing molecules are the main protectors against ROS in living organisms. The thiol group is found in every cysteine residue, however not every cysteine-containing peptide is capable to neutralize ROS. Protonation processes can be viewed either from the point of proton association or proton dissociation. In the first case protonation constants (K), in the latter case dissociation (ionization) constants (K_a)

characterize the process. The logarithms of the obtained protonation constants correspond to the negative logarithms of dissociation constants, namely $pK_{a1}=\log K_3$, $pK_{a2}=\log K_2$ and $pK_{a3}=\log K_1$. (Mazák K. and Noszál B., 2016).

Reactive cysteines in peptides generally have a pK_a value of 7 or lower, compared to the relatively higher pK_a value of the amino acid cysteine (pK_a = 8.33) (Leslie B. Poole, 2014). The surrounding microenvironment of the cysteine is the explanation of this decrease in pK_a. It allows the thiol (-SH) to get rid of its H^+ easier, than in case of cysteine, resulting in the relative abundance of the thiolate ($-S^-$) form near physiological pH (Hoffman et al., 2015). Thiolate functional groups can be oxidized directly in redox reactions, forming disulfide (-SS-) bonds while the ROS are reduced and thus neutralized. The protonation and oxidation propensity of thiolate groups depend on the electron density around the sulfur atom. The expected relationship between redox and protonation properties has been studied and reported for various thiolates (Keire et al., 2008, and Mirzahosseini A. and Noszál B., 2014).

Glutathione (GSH) is one of the well-known members of easily oxidizable cysteine containing endogenous antioxidants. GSH depletion and GSH-related enzyme deficit are involved in the pathology of several neuropsychiatric and neurodegenerative diseases, such as autism, schizophrenia, bipolar disorder, Parkinson's, and Alzheimer's disease. Moreover, the redox imbalance of glutathione may be a primary cause of these disorders (Feng Gu et al., 2015). As a conclusion it is obvious, that different types of thiolate-containing molecules (especially glutathione) are indispensable factors to protect cells against harmful oxidative stress and to preclude several diseases.

1.3. The importance of microspecies

Most thiolate-containing molecules (for example gluthatione, mercaptoethanol, cysteamine, conotoxins) are multibasic ones, i.e., they contain not only a thiolate, but further protonating groups, such as amino, carboxylate, imidazole, phenolate, etc. groups, resulting in various molecule-specific protonation schemes. The different protonation states of the microspecies of each molecule result in different physico-

chemical properties. We chose for our studies mercaptoethanol (MSH), mercaptoethanol disulfide (MSSC), cysteamine (CSH) and cystamine (CSSC), as relatively simple model compounds. In the redox reactions heterodisulfides were also produced in the solutions (for example MSSC in the mercaptoethanol – cysteamine system). For the thorough characterization of these processes, microscopic parameters are needed, which have earlier been established for protonation constants (Szakács Z., Noszál B., 1999. and Mirzahosseini A., Noszál B., 2014), redox equilibrium constants (Mirzahosseini A. et al., 2015), and redox potentials (Mirzahosseini A., Noszál B., 2016).

1.3.1. Protonation processes

Protonation processes can be considered at a microscopic and at a macroscopic level. If a molecule has only one basic moiety, the macroscopic and microscopic descriptions are essentially the same, we can associate one microscopic species to each macroscopic form. For illustration see MSH or MSSC on Figure 1.

In case of two basic moieties in a molecule, the protonation scheme depends on the quality and p*K*a values of the protonating groups. If the basicities of the two groups differ by at least 3 p*K*a units (a conventional, arbitrary limit, which will decrease along with the increasing determination accuracy of the protonation constants), the protonation processes take predominantly place in a stepwise fashion, in which major and minor protonation pathways exist, and microconstant values of the major protonation pathway are very close to some macroconstants. If the inherent basicities of the two sites are comparable, all macro- and microconstant values are significantly different. If the molecule is symmetrical (see CSSC on Figure 1) some microconstants can be calculated directly from the macroconstants, without any additional (e.g., spectroscopic, or other group-selective) information.

If the p*K*a-s of the two groups do not have a difference of at least 3, the protonation processes occur in a significantly overlapping fashion. This results in a protonation scheme, like that of CSH in Figure 1. In this scheme 3 macroscopic forms exist with 4

distinct microscopic species, since two microspecies (*g* and *h*) contain the same number of protons, however, at different sites, these latters are therefore protonation isomers.

The protonation propensity of a group is affected by the protonation state of the neighbouring basic moieties in the molecule as well if there is interaction between the moieties. As an example, we can see the protonation scheme of CSH on Figure 1, where the amino group has different microconstants, depending on whether the thiolate is protonated or not (see species *h* and *f*, and the related, respective microconstants 9.55 and 10.85).

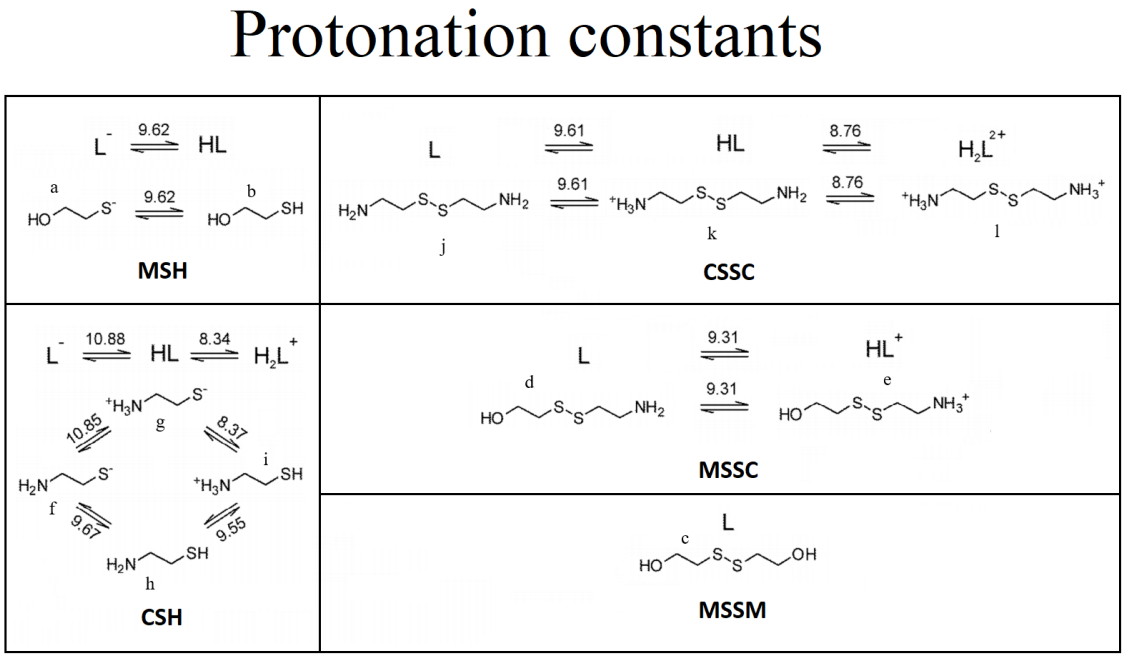

Figure 1. Summary scheme of acid-base equilibria and the related protonation constants in log unit of MSH, CSH, CSSC, MSSC and MSSM. Note that CSH has microscopic protonation constants therefore protonation isomers, whereas MSSM does not have any acid-base function within the customary pH range (Mirzahosseini A. et al, 2018).

1.3.2. Redox processes

The reaction between a disulfide and a thiol can be divided into two steps. The first step results in heterodisulfide formation, and the second step results in the formation of the other homodisulfide, relative to the original thiol, depicted in Figure 2

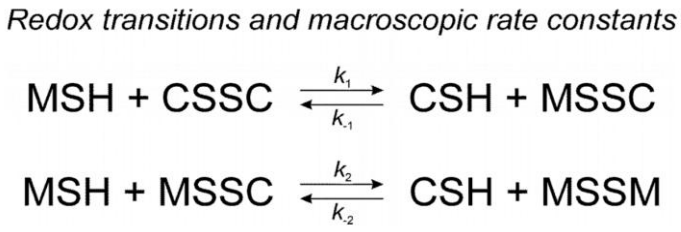

Figure 2. Summary scheme of redox transitions and related pH – dependent macroscopic rate constants (Mirzahosseini A. et al, 2018).

It is well-known, that it is the thiolate bearing species that participates in S_N2-mediated redox reaction with the disulfide (Szajewski RP., Whitesides GM., 1980; Nagy P. 2013).

Considering all the possible combinations of the differently charged thiolates and disulfides that can react (Figure 1), we can distinguish 6 reactions for the above system, including 12 pH – independent microscopic rate constants (Figure 3).

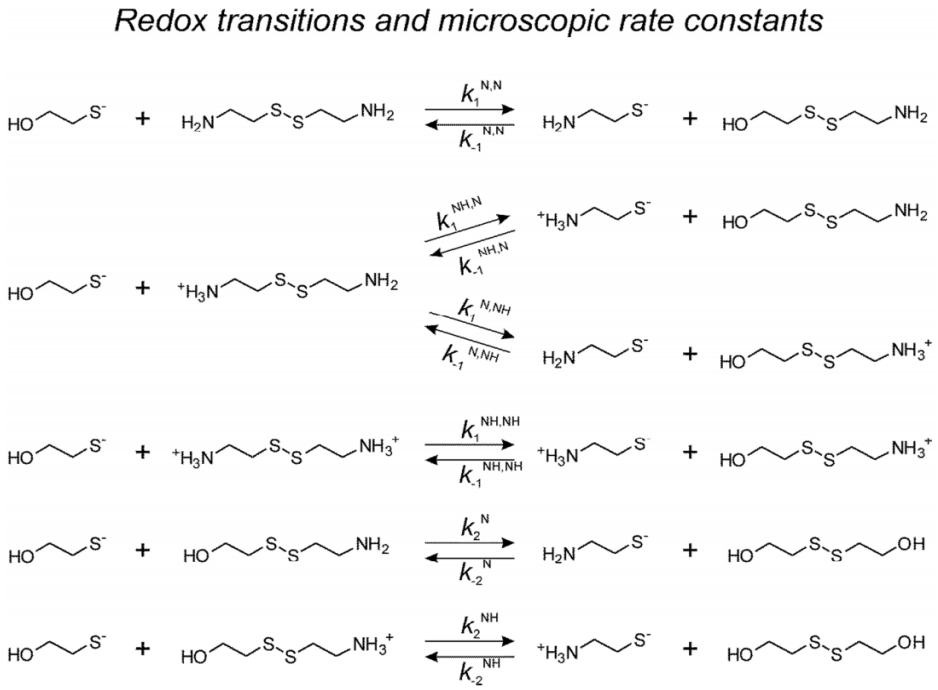

Figure 3. Summary scheme of redox transitions and pH – independent microscopic rate constants. The details of the notation are in chapter Discussion. (Mirzahosseini A. et al, 2018).

The complexity of this reaction system increases exponentially with the number of basic moieties, which is why in our study we used model compounds with the minimum number of protonation sites that still makes the investigation meaningful.

1.4. Beyond protection: tertiary structure of peptides

Besides this protective function against ROS, disulfide bonds are important factors to provide a tertiary structure for proteins. Disulfide bonds are found in nearly one third of the proteins in a eukaryotic cell. Proper disulfide bonds ensure stability to a protein, decreasing the number of further entropic choices of the folding progression toward the native state (Kastin AJ., 2013).

Without disulfide bonds many of the proteins would be unable to fulfil their tasks in organisms. Thus, the lack of the well-formed disulfide bonds, even in only one specific amino acid could result in misfolding which could be fatal. Several diseases are caused by misfolding, such as prion-related disorder, amyotrophic lateral sclerosis or tauopathy (Maria Francesca Mossuto, 2013).

After our first objective of modelling the oxidation kinetics of GSH with relatively simple model compounds (mercaptoethanol, cysteamine and their disulfides) we sought to examine the effects of physico-chemical properties (especially pK_a) on native disulfide bond formation patterns in peptides.

The reactivity of a thiol groups depends on the electron density around the sulfur atom, that can be affected through-space or through-bond interactions, which will define the acid-base and the redox properties of the group. The closer is an electron-withdrawing or donating group located to the -SH group, the more it influences its acid-base and redox properties. Protonation of a molecule is one of the most significant events that can change the electron distribution. Protonation certainly increases the electron-withdrawing effect of any site, no matter how much electron-withdrawing or –donating the site was before protonation. Thus, the lower the pH, the smaller the electron density around the sulfur, which results in a less oxidizable thiolate. Even protonation isomers have different properties, because not only the number of the basic moieties and the associated protons, but also, the location of the protonation sites influence the characteristics of the reactive molecules.

1.5. Conotoxins: the example of nature's diversity

Conotoxins, a group of neurotoxic peptides, isolated from the venom of the marine cone snail (genus *Conus*), have been chosen in this work to examine the disulfide forming patterns of peptides. The main reason we selected this class of peptides is their relatively small size; they consist only of 10 - 60 amino acid residues, making them one of the smallest peptides in nature that contain multiple disulfide bonds. The venom of the marine predatory cone snail has evolved for prey capture and self-defence. The success of the venom is provided by hundreds of bioactive peptides. Conotoxins are of interest to neuroscientists and drug developers due to their potency and selectivity. Now well over 10.000 conotoxin sequences were published, showing the diversity of nature (Ai-Hua Jin et al., 2019). The conotoxin family classification is based on the target type and the pathway of action and thus it can be divided into 12 classes (α-, γ-, δ-, ε-, ι-, κ-, μ-, ρ-, σ-, τ-, χ-, ω-conotoxins) (Harry Morales Duque et al., 2019). Conotoxin structures can be distinguished depending on the number of cysteines and therefore the number of disulfide bonds. They can be linear peptides, without a disulfide bond, like conantokins, or may possess between one and five disulfide bonds (Eline K.M. Lebbe, Jan Tytgat, 2016). Loop class is a category used to divide the α-conotoxin family, the most studied one, into subclasses (Victor Tsetlin et al., 2009). In this respect, the classification may be based on the amino acid number distribution among Cys (C1C2*m*C3*n*C4), where *m* and *n* are loops (Kalyana B Akondi, et al., 2014). There are three options for the forming of the disulfide bonds: the globular connectivity (C1-C3 and C2-C4), the ribbon connectivity (C1-C4 and C2-C3) and the beads connectivity (C1-C2 and C3-C4) (Bodil B. Carstens et al., 2016).

We used in our experiments a reduced derivative of α-conotoxin MI with the sequence of GRCCHPACGKNYSC. (See Figure 4 for primary structure) The native disulfide pattern in oxidized α-conotoxin MI was determined by Gray et al. in 1983. The solution structure of α-conotoxin MI was described by Gouda et al. in 1997 with ^{1}H NMR spectroscopy and molecular dynamics simulation. They confirmed Gray's proposed structure, with a 3_{10} helix and type I β-turn motif. According to their measurements, the tyrosine residue is placed in the centre of the structure, the N-terminal is looped back close to the C-terminal and the lysine and arginine side chains point outward.

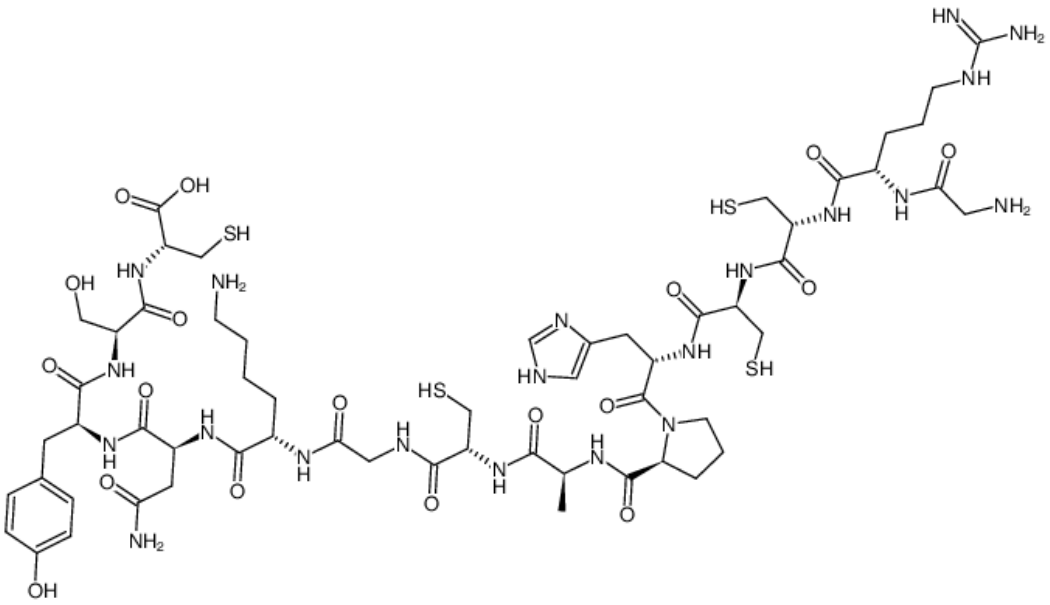

Figure 4. Primary structure of the α-conotoxin's derivative MI (with the sequence of GRCCHPACGKNYSC)

2. Objectives

Our main objectives were to investigate what kind of features and reaction conditions influence the rate and quality of the disulfide bridge formation.

2.1. Reaction kinetics and reaction rate constants of thiol oxidation

In this study our primary aim was the investigation of the pH – reaction velocity relation, secondarily the definition of species – specific kinetic constants (which are pH-independent parameters) for the thiolate – disulfide transition reactions, using the simplest model compounds, mercaptoethanol – cystamine, mercapthoethanol-disulfide and cysteamine. With these models we were able to ascertain the through-bond influence of a two-carbon-distance protonated amino and hydroxyl group for the thiol-oxidation, which can be used for an approximation of glutathione's redox attribution.

2.2. Connection between pK_a and disulfide bonds in a derivative of α-Conotoxin MI

After the characterisation of the reduced α-conotoxin-MI NMR spectra, we wanted to determine the species- and site-specific constants, including 4 thiolate pK_a values. With these pK_a values our purpose was to find out how pK_a values affect the disulfide bond formation. Based on our hypothesis, the thiolate groups with the highest protonation constants and therefore highest oxidation propensities will form disulfide bonds first, unless a strong alternate conformational preference exists.

3. Results

3.1. Thiol - disulfide reactions

3.1.1. Data analysis

For the characterization of thiolate – disulfide reactions between MSH – CSSC and MSSM – CSH we used quantitative ^{1}H NMR. The solvent in every case was an aqueous solution with H_2O: D_2O, 95: 5 V/V%, with 0.15 mol / dm^3 ionic strength. NMR spectra were recorded on a Varian 600 MHz spectrometer at 298 K. pH values were determined by internal indicator molecules, optimized for NMR.

The exact concentrations of the reagents before the reaction were determined by high precision gravimetric analysis. D_2O, acetone (as chemical shift reference), and a pH indicator (sodium acetate or imidazole), which also served as a concentration standard, were added to the solutions. The pH of the solutions was adjusted with aqueous phthalate buffer (0.1 mol / dm^3) and hydrochloric acid or sodium hydroxide. The concentration of the reagents and products as a function of time, can be calculated from NMR spectra after the assignment (see Figure 5 for details), and integration.

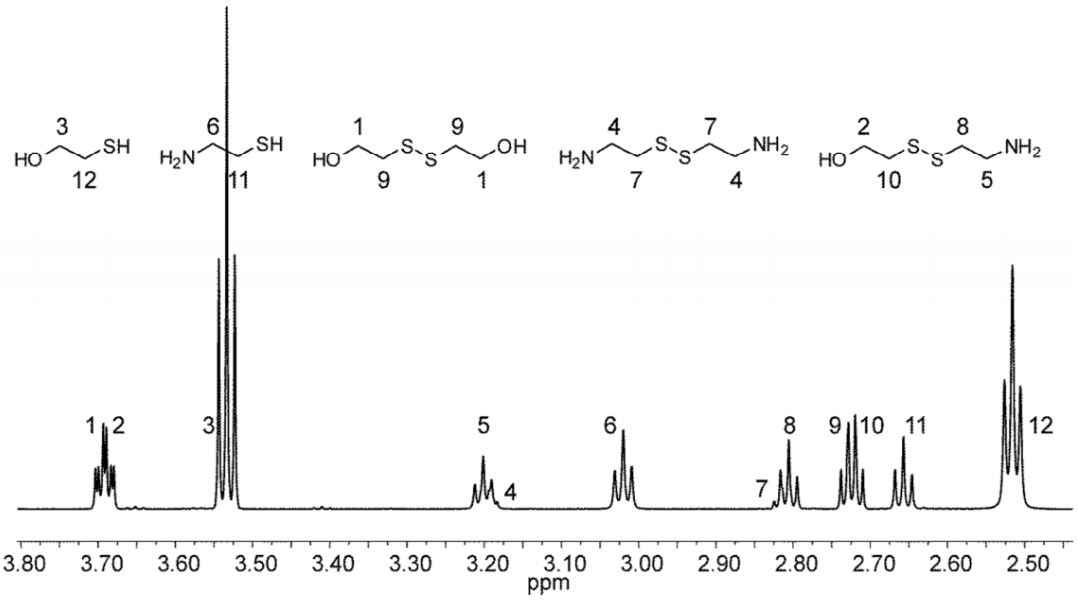

Figure 5. 1H NMR spectrum of the 12 different methylene peaks of the five different compounds (from left to right: MSH, CSH, MSSM, CSSC and MSSC) on pH = 4.8. (Mirzahosseini A. et al, 2018)

We could integrate the peaks between 4 < pH < 6, because below pH = 4, the reaction was too fast compared to the time needed for one spectrum, whereas above pH = 6 the transition took several days and weeks. We have got 10 sets of measurements for the MSH + CSSC reaction, and 7 sets of measurements for the MSSM + CSH reaction on different pH-s. One set of measurements included 15 – 30 spectra, resulting in 75 – 150 concentration data on one pH, as a function of time.

3.1.2. pH-dependent rate constants

ACD/NMR Processor Academic Edition v12.01 software package and Origin Pro 8 have been used for NMR spectra procession and data analysis. All the possible reactions between the microspecies and their rate constants are depicted in Figure 3. The rate constants are indexed as follows: the superscript indicates the protonation state of the amino group in the reactants (N means NH_2 and NH means NH_3^+), the subscript signs the forward / reverse and first - / second – step reactions. Note that in the case of cystamine, the monoprotonated microspecies is asymmetrical, resulting in two potential reactions. The thiolate can react with two non-identical sulfur atoms in the monoprotonated CSSC, which obviously will have different reactivities. The two rate constants will also differ, here we named these $k_1^{NH,\,N}$ and $k_1^{N,\,NH}$.

Applying the results of the 17 sets of measurements, regression analysis was performed for both directions (forward and reverse), for each reactant in every set, using the equation of exponential decay:

(1) $[reactant] = A * e^{\frac{-t}{\tau}} + B$

Where A is the initial concentration of the reactant, e is Euler's number, τ is the exponential time constant, and B is the correction factor. The time constant τ is the amount of time, that an exponentially decaying quantity (i.e., concentration) takes to decay by a factor of $1/e$. $1/e$ is approximately 0.368, so τ is the amount of time that the concentration takes to decay to 36.8% of its original amount. Correction factor B signs the concentration of the reactant after the reaction, in the equilibrium. For the goodness-of-fit see Figure 6. To calculate the apparent rate constant, the following transformations were performed: only the first step of the reaction affects the

consumption of the reactants at t = 0 s. These can be formulated for forward and reverse directions as follows:

(2) $v_1 = k_1[MSH]_0[CSSC]_0 = \frac{-d[MSH]}{dt} = \frac{-d[CSSC]}{dt}$

(3) $v_{-2} = k_{-2}[MSSM]_0[CSH]_0 = \frac{-d[MSSM]}{dt} = \frac{-d[CSH]}{dt}$

Where the subscript zero after the square bracket signifies initial concentration. The derivative terms of equation (2) and (3) were acquired from the derivative form of equation (1):

(4) $\frac{-d[reactant]}{dt} = \frac{A}{\tau} e^{\frac{-t}{\tau}}$

A/τ can be calculated from fitted parameters at t = 0 s. From v_1 and v_{-2} k_1 and k_{-2} are definable. The determination of k_{-1} and k_2 requires the redox equilibrium constants, measured and numerated from equilibrium concentrations:

(5) $K_{1C}^{REDOX} = \frac{[CSH]_e * [MSSC]_e}{[MSH]_e * [CSSC]_e}$

(6) $K_{2C}^{REDOX} = \frac{[CSH]_e * [MSSM]_e}{[MSH]_e * [MSSC]_e}$

These equilibrium constants, (5) and (6), are conditional ones, thus there is C in the subscript, and the letter e subscript sign after the square bracket indicates equilibrium concentration.

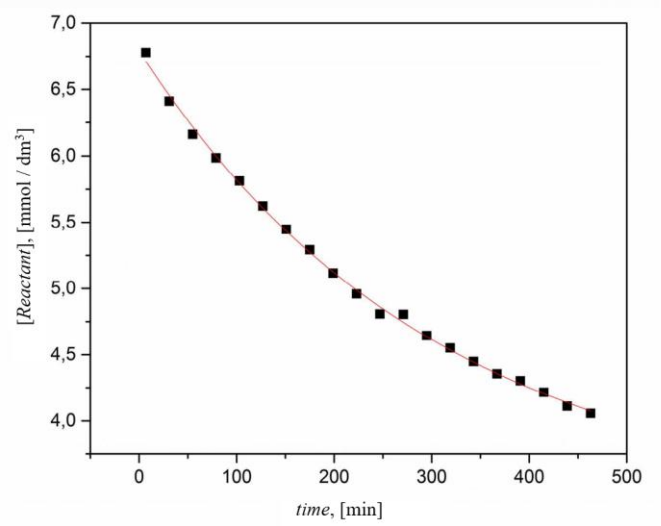

Figure 6. The fitted exponential decay of mercaptoethanol reactant at pH = 4.62. (Mirzahosseini A. et al, 2018)

3.1.3. pH independent rate constants

The microscopic rate constants were determined from rate equations, composed of microspecies concentrations, and microscopic rate constants. For assignment details see Figure 1. In case of the reaction between MSH and CSSC, considering the three microspecies of CSSC (j, k and l), equation (2) can be written as the sum of all contributing real reaction velocities. CSH has two different protonation states, resulting in a sum of two reactions in case of the reaction between MSSM and CSH. Reaction rates v_1 and v_{-2} are as follows:

(7) $v_1 = k_1[MSH][CSSC] = k_1^{N,N}[a][j] + \left(k_1^{NH,N} + k_1^{N,NH}\right)[a][k] + k_1^{NH,NH}[a][l]$

(8) $v_{-2} = k_{-2}[CSH][MSSM] = k_{-2}^{N}[f][c] + k_{-2}^{NH}[g][c]$

Rearranging (7) and (8) equations, the connection between the micro and macro rate constants is getting clear in equations (9) and (10):

(9) $k_1 = \chi_a * \left[\left(k_1^{N,N}\chi_j\right) + \left(k_1^{NH,N} + k_1^{N,NH}\right)\chi_k + \left(k_1^{NH,NH}\chi_l\right)\right]$

(10) $k_{-2} = \chi_c(k_{-2}^{N}\chi_f + k_{-2}^{NH}\chi_g)$

Where χ is the mole fraction of the microspecies in its subscript. The mole fraction values were calculated from the protonation constants, for instance:

(11) $\chi_a = \frac{[a]}{[a]+[b]} = \frac{1}{1+K_1*[H^+]}$

(12) $\chi_g = \frac{[g]}{[f]+[g]+[h]+[i]} = \frac{k^N*[H^+]}{1+K_1*[H^+]+K_1*K_2*[H^+]^2}$

The microscopic $k_{-1}^{NH,NH}$ and k_2^{NH} rate constants were calculated using the microscopic, species–specific redox equilibrium constants. The microscopic redox equilibrium constants are defined in equations (13) and (14):

(13) $K_1^{REDOX,a-l} = \frac{k_1^{NH,NH}}{k_{-1}^{NH,NH}} = \frac{[g][e]}{[a][l]} = \frac{[CSH]_e\chi_g[MSSC]_e\chi_e}{[MSH]_e\chi_a[CSSC]_e\chi_l} = \frac{K_{1C}^{REDOX}*\chi_g\chi_e}{\chi_a\chi_l}$

(14) $K_2^{REDOX,a-e} = \frac{k_2^{NH}}{k_{-2}^{NH}} = \frac{[g][c]}{[a][e]} = \frac{[CSH]_e\chi_g[MSSM]_e}{[MSH]_e\chi_a[MSSC]_e\chi_e} = \frac{K_{2C}^{REDOX}*\chi_g}{\chi_a\chi_e}$

The conditional equilibrium constants were determined at different pH values approaching from both directions, resulting:

(15) $log\ (K_1^{REDOX,a-l}) = 1{,}91\ \pm\ 0{,}07$

(16) $$log\ (K_2^{REDOX,a-e}) = 0{,}77\ \pm\ 0{,}09$$

For calculated macroscopic and microscopic rate constants see Table 1. For the change of apparent rate constant as a function of pH see Figure 7.

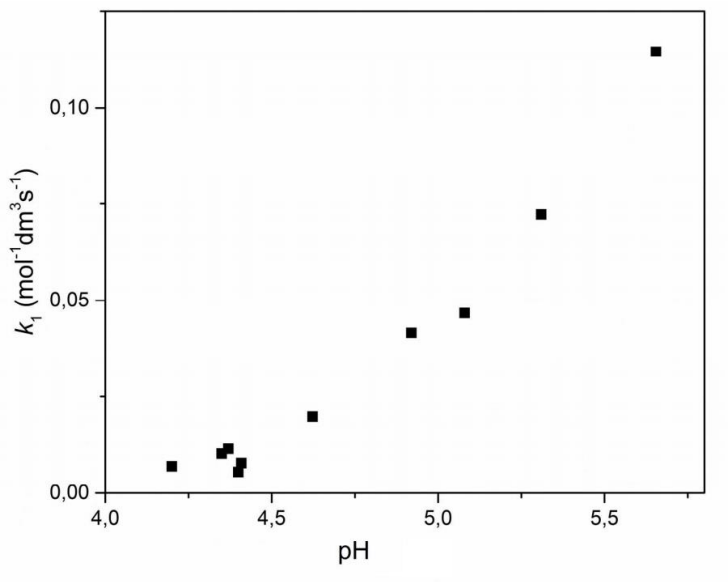

Figure 7. The apparent rate constant, k_1 as a function of pH. (Mirzahosseini A. et al, 2018)

Table 1. The macroscopic / apparent and microscopic rate constants are presented in log units. The dimension of the rate constants is mol^{-1}*dm^3*s^{-1}. (Mirzahosseini A. et al, 2018)

Forward direction			Reverse direction		
pH	logk_1	log$k_1^{NH.NH}$	pH	logk_{-2}	logk_{-2}^{NH}
4.20	-2.385	2.553	4.30	-3.097	0.573
4.35	-1.990	3.300	4.42	-3.503	0.811
4.37	-1.940	3.330	4.52	-3.135	1.200
4.40	-2.260	2.990	4.82	-2.650	1.059
4.41	-2.109	3.122	5.04	-2.488	0.964
4.62	-1.702	3.315	5.05	-2.367	0.540
4.92	-1.382	3.339	5.24	-2.395	0.740
5.08	-1.385	3.175			
5.31	-1.096	3.234			
5.66	-0.976	3.009			

The consequently determined microscopic rate constants are depicted in Figure 8.

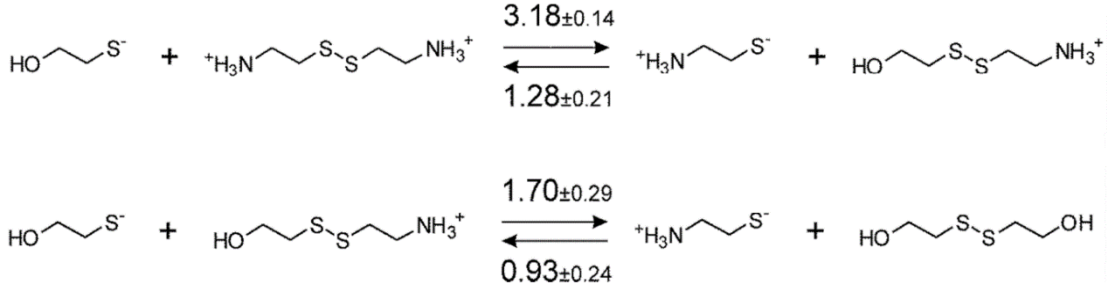

Figure 8. The determined $k_1^{NH,NH}$, $k_{-1}^{NH,NH}$, k_2^{NH} and k_{-2}^{NH} microscopic rate constants in log units with the corresponding arrows. The dimension of the rate constants is $mol^{-1}*dm^3*s^{-1}$. (Mirzahosseini A. et al, 2018)

3.2. Determination of the protonation constants and structure of reduced conotoxin

3.2.1. NMR – pH titration of the α-Conotoxin MI derivative

The peptide was titrated in D_2O solution at 298 K and 0.15 mol / dm^3 ionic strength, the pH was adjusted with DCl and NaOD. The methyl signal of internal DSS was used as a chemical shift reference. A D_2O solution was used to perform the titration since the methylene ^1H signals that could be used for the evaluation are close to the water signal and are often suppressed in ^1H measurements with solvent suppression. During the titration, the protonating group had the biggest affect in chemical shift to the nearest H atom's signal. Therefore, these proton signals have been used for the determination of the pK_a values. When βH signals were not observable, αH signals were used as alternatives (see Figure 9 for details). The reading of the overlapping signals was supported with ^1H – ^{13}C HSQC and COSY measurements.

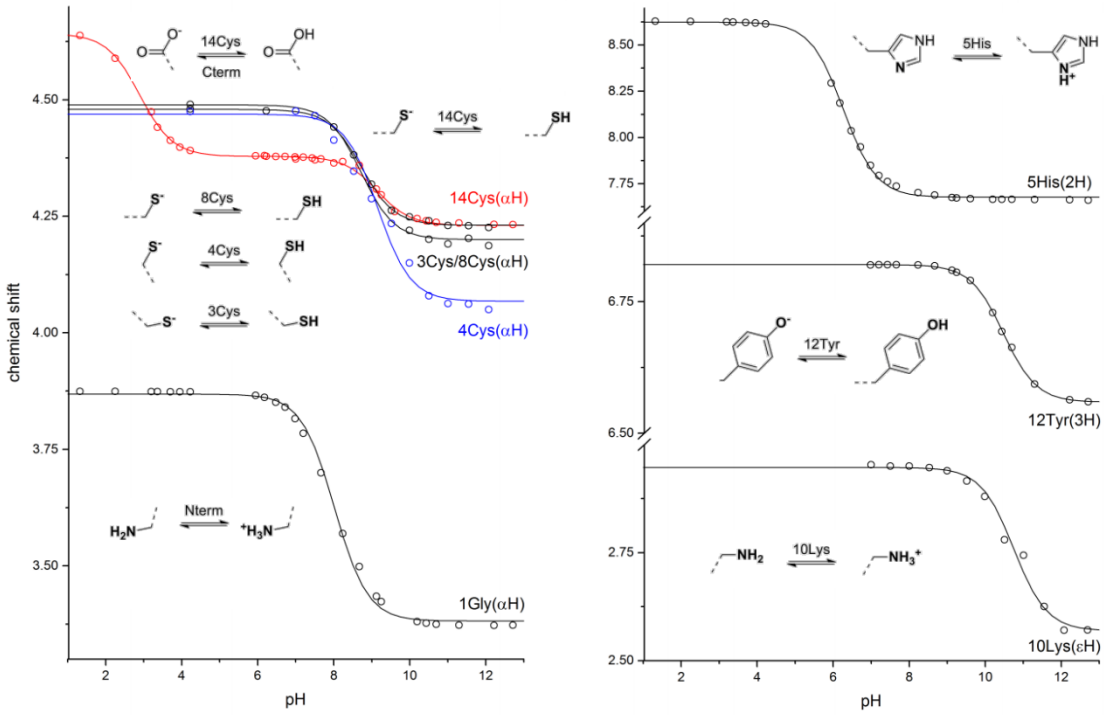

Figure 9. The 1H NMR titration data and fitted curves of the peptide. (Faragó Z. et al, 2021)

Due to the large covalent distance between the protonating groups in the peptide, it can be concluded that none of the basic moieties can influence the protonation of any of the other basic moieties. Therefore, all basic moieties protonate independently. In case of 14Cys, the pK_a values of the thiolate and the carboxylate protonations are so different that they can be regarded as independent monoprotic sites, despite the small covalent distance. The pK_a values are in Table 2.

Table 2. The pK_a values of α-Conotoxin MI peptide (Faragó Z. et al, 2021)

	pK_a value
3Cys or 8Cys	8.53
8Cys or 3Cys	8.52
4Cys	8.97
14Cys	8.91
Nterm	7.87
5His	6.24
10Lys	10.41
12Tyr	10.16
Cterm	3.11

3.2.2. 2D NMR spectra

A 0.5 mmol / dm^3 aqueous solution (containing 5 V/V% D_2O) of the peptide was prepared at pH 4.5 (298 K and 0.15 mol / dm^3 ionic strength), for the 3D structure determination. pH 4.5 was chosen because the average relative charge – pH curve has a plateau at this point. The peptide occurs predominantly in a +3 charged state at pH = 4.5 (See Figure 10).

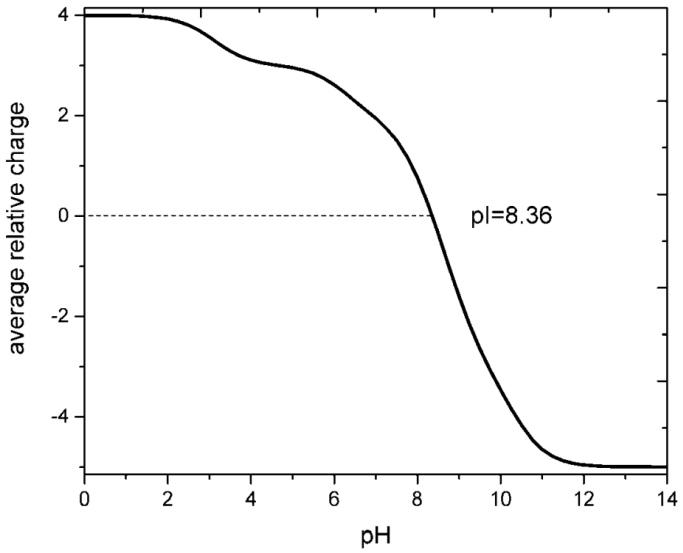

Figure 10. The calculated average charge of the peptide as a function of pH. (Faragó Z. et al, 2021)

The entire assignment (see Table 3) of the peptide was performed using NOESY and COSY spectra (Figure 11) and confirmed with TOCSY spectrum. The chemical shift reference was the methyl signal of the internal DSS in the solution.

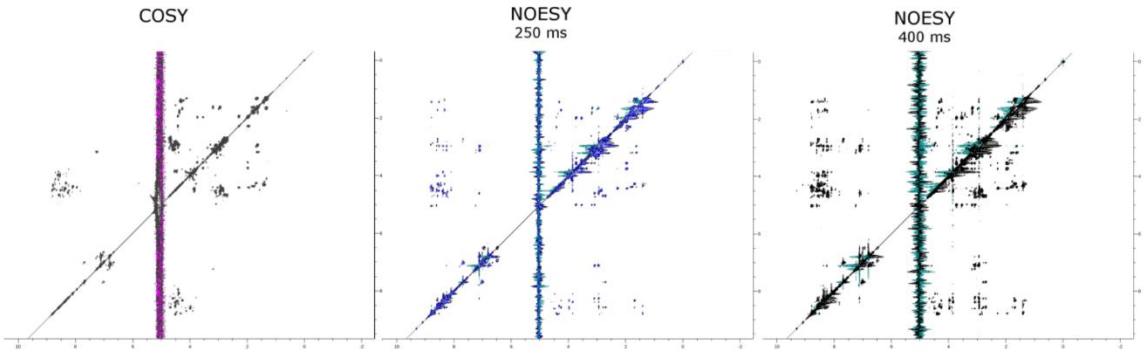

Figure 11. COSY and TOCSY spectra (with two different mixing time, 250 ms and 400 ms) (Faragó Z. et al, 2021)

Table 3. The assignment table of the ^{1}H signals at pH 4.5. (Faragó Z. et al, 2021)

	NH	αH	βHa	βHb	others			
1Gly		3.85						
2Arg	8.78	4.37	1.76	1.83	1.63(γ)	3.18(δ)	7.24(ω)	
3Cys	8.80	4.50	2.89					
4Cys	8.73	4.46	2.84					
5His	8.61	4.99	3.09	3.18	7.63(2H)	6.96(5H)		
6Pro		4.42	1.94	2.29	1.97(γ)	3.54(δa)	3.75(δb)	
7Ala	8.78	4.33	1.41					
8Cys	8.52	4.51	2.94					
9Gly	8.60	3.98						
10Lys	8.33	4.26	1.68	1.69	1.29(γa)	1.34(γb)	1.63(δ)	2.94(ε)
11Asn	8.57	4.68	2.70	2.79				
12Tyr	8.26	4.59	2.94	3.09	7.12(2.6H)	6.80(3.5H)		
13Ser	8.38	4.47	3.85					
14Cys	7.99	4.39	3.10	3.25				

3.2.3. CD measurements

After the titration of the peptide the circular dichroism spectrum of the peptide was recorded at selected pH values to cover the entire pH region of the protonation (See Figure 12).

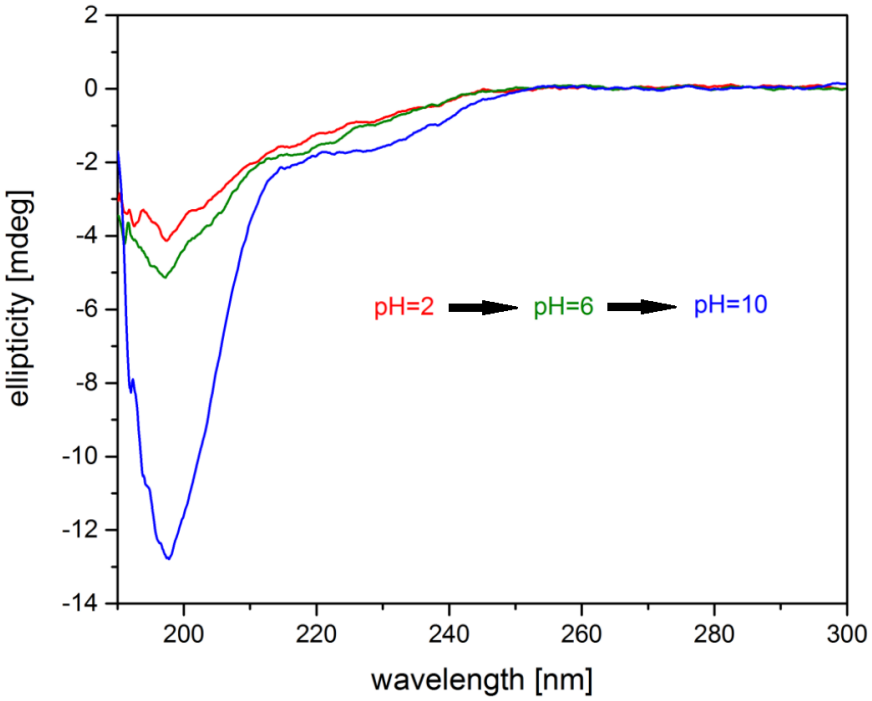

Figure 12. CD spectra of the peptide at pH values 2, 6 and 10. At pH 8 the solution was opalescent because pI = 8.36. (Faragó Z. et al, 2021)

3.2.4. Structure determination

2D NOESY spectra were studied for structure determination, at pH 4.5 medium, with CcpNmr Analysis V2 and ARIA. The structure refinement created 7 alternative structures, of which the best mean structure is in Figure 13. We also attempted to determine the structure of the peptide at a high pH value, where every protonating group is deprotonated (except for the arginine guanidinium), resulting in an average charge of -5. Molecular dynamics simulations were used for the conformation search of the peptide (with +3 and -5 charges). Results are depicted in Figure 13.

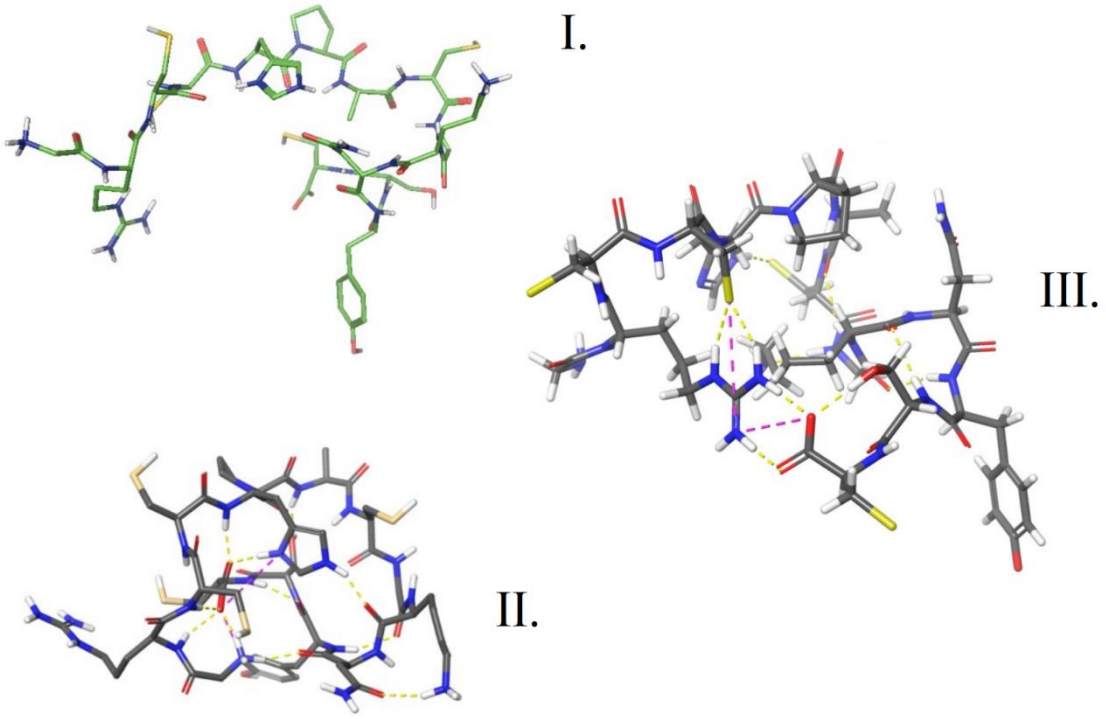

Figure 13. Solution structures of the reduced α-Conotoxin MI, with charge +3 (I. and II. structure) and -5 (III. structure). Structure I. has been determined with NMR, structure II. and III. with molecular dynamics simulations. Pink dashed lines indicate ionic interactions, yellow dashed lines indicate H-bonds. (Faragó Z. et al, 2021)

4. Discussion

4.1. Thiol – disulfide reaction rates

The pH-dependent apparent rate constants were determined as a function of pH for cystamine / mercaptoethanol redox system under acidic conditions (4 < pH < 6) (see Figure 7) The apparent rate constant shows an exponential – like rise with the pH, as the relative abundance of the thiolate species increases. The curve of this function is expected to be sigmoidal because the mole fraction of the thiolate form is approaching its maximum under extremely basic conditions. $k_1^{NH,NH}$, $k_{-1}^{NH,NH}$, k_2^{NH} and k_{-2}^{NH} microscopic rate constants characterize the reactions between reagents with the fully protonated sidechains. The reaction time below pH 4 took weeks, above pH 6 took less than an hour, resulting in too fast reactions for NMR measurements. The very fast kinetics might be followed by stopped – flow techniques. Measurements under basic conditions would afford to define $k_1^{N,N}$, $k_{-1}^{N,N}$, k_2^{N} and k_{-2}^{N}, while measurements in intermediate pH values would afford to define $k_1^{NH,N}$, $k_{-1}^{NH,N} \wedge k_{-1}^{N,NH}$. Changing the pH alters the concentration of the reactant species and changes the protonation state of the side – chains too. For rough-approximation we can assume that the pH dependence of the rate constants for thiolate – disulfide processes are mostly explicable with the concentration of the thiolate form: under basic conditions the abundance of the reactive thiolate forms increases, the apparent rate constants extend, the reactions are getting faster.

However, as expected, there are differences between the reactivity of the microspecies. Comparing the microscopic rate constants, $k_1^{NH,NH}$, $k_{-1}^{NH,NH}$, k_2^{NH} and k_{-2}^{NH} (see Figure 8) we can assume that $k_{-2}^{NH} < k_{-1}^{NH,NH} < k_2^{NH} < k_1^{NH,NH}$. Considering the reasons of the differences, we can state three explanations. The inductive effect differences in the thiolate reactant, the inductive effect differences in the disulfide reactant and coulombic effect differences.

The inductive effect differences in the thiolate reactants explain $k_{-1}^{NH,NH} < k_2^{NH}$relation. The thiolate-bearing mercaptoethanol (microspecies *a*) reacts much more readily with the hetero-disulfide than the thiolate-bearing cysteamine (microspecies *g*), because the

protonated amino group has stronger -I effect on the electron density of the thiolate group, than a hydroxyl group, resulting in a weaker nucleophilic reagent.

The inductive effect differences in the disulfide reactants explain $k_2^{NH} < k_1^{NH,NH}$, and $k_{-2}^{NH} < k_{-1}^{NH,NH}$ relations. Comparing the reactivity of microspecies *c*, *l* and *e*, we can state that mercaptoethanol-disulfide (microspecies *c*) is the less reactive disulfide and the fully protonated cysteamine (microspecies *l*) is the most reactive disulfide, because the protonated amino group has stronger -I effect on the electron density of the disulfide linkage, than hydroxyl group. It makes microspecies *l* the most electrophilic, and microspecies *c* the less electrophilic reagent.

Beyond the inductive differences, there is a more than two orders of magnitude difference between k_{-2}^{NH} and $k_1^{NH,NH}$. This huge difference is evident if we consider that $k_1^{NH,NH}$ characterizes a reaction between a doubly positive and a negative ion, whereas k_{-2}^{NH} characterizes a reaction between a neutral molecule and a zwitterion.

4.2. Protonation state-dependent structure of reduced conotoxin

4.2.1. pK_a values and disulfide bonds

The protonation constants of the reduced peptide clearly indicate that the thiols with similar pK_a values are going to form disulfide linkages in the native form. This supports the theory, that the cysteines with the larger protonation constant (and therefore highest oxidizabilities) tend to form disulfide bonds first. Thiolate basicites correlate with thiolate redox potentials (Mirzahosseini A and Noszál B, 2016). Based on this close correlation we can calculate the group – specific standard redox potentials for the four cysteine residues: 3Cys and 8Cys E^o = -0.35 ± 0.01 V/mol; 4Cys E^o = -0.377 ± 0.015 V/mol and 14Cys E^o = -0.374 ± 0.005 V/mol. Figure 14 shows the correlation between pK_a values (log$K$) and E^o.

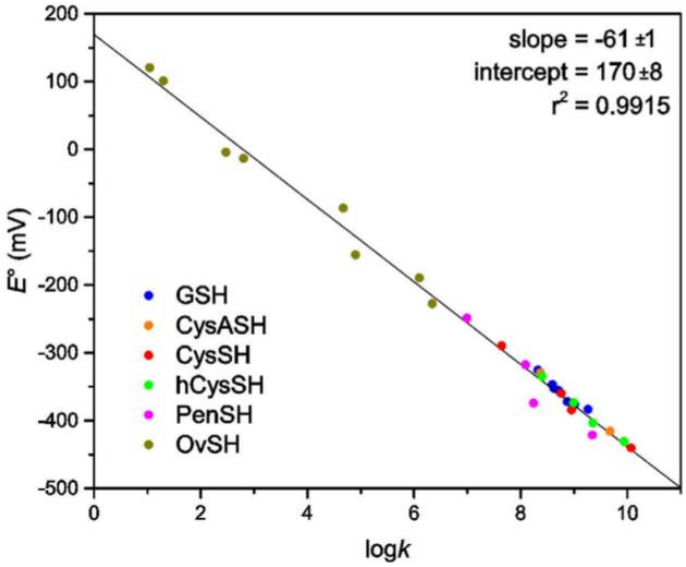

Figure 14. The correlation between species-specific standard redox potentials and the species-specific thiolate protonation constants for the various thiols. (Mirzahosseini A. and Noszál B, 2016).

4.2.2. 3D structure

It was obvious from the CD and NMR measurements and molecular dynamics simulations that the peptide at pH 4.5 does not occur in any classical secondary structure. Instead of this, the reduced peptide forms a loop-like 3D structure, with the tyrosine residue positioned in the centre, and brings the thiol groups into the vicinity of each other. This structure is like the oxidized α-Conotoxin MI, with the same charge. The completely deprotonated form of the reduced peptide at pH 12.5 demonstrates an untethered structure that locates the negatively charged groups in distant positions (Figure 13). The peptide structure between 4.5 < pH < 12.5 can be approximated by a structure that leads from the structure at pH 4.5 to the structure at pH 12.5. Based on the NMR signals of the products, it could be observed that approaching high pH values (above 10) a mixture of oxidized products is formed, due to the oxidation of the peptide by air. The oxidation of the fully deprotonated peptide results in a mixture of various oxidized structures (bead, ribbon, globular).

5. Conclusions

Thiol oxidation was examined on CSSC – MSH and MSSM – CSH systems to model the redox properties of glutathione with relatively simple and easier to handle molecules. Measuring the concentrations of the reactants and products (for instance see Figure 6), with quantitative ^{1}H-NMR and using a new method for data processing (equations (1) - (6)), we have determined pH-dependent apparent rate constants between 4 < pH < 6 (see Figure 7 and Table 1). Based on the calculated relative abundance of microspecies and equilibrium constants, pH independent microscopic rate constants have been defined for $k_1^{NH,NH}$, $k_{-1}^{NH,NH}$, k_2^{NH} and k_{-2}^{NH} (for details see equations (7) – (16), for results, see Figure 8). The curve of the apparent rate constants as a function of pH shows an exponential – like rise under acidic conditions (4 < pH < 6) although it is expected to be a sigmoidal under basic conditions. The microscopic rate constants were significantly different from each other.

Further measurements under basic conditions could be useful in the future to quantify more microscopic rate constants and to observe the sigmoid curve of the apparent rate constant – pH function. However, it is necessary to use other technics (for instance stopped flow method) for these goals, because the rate of the reactions gets too fast for NMR measurements.

In other experiments we studied how physico – chemical properties of the thiol groups affect the disulfide bond formations. For the investigation the reduced derivative of α-conotoxin MI was chosen (for primary structure see Figure 4). After ^{1}H-NMR, ^{1}H – ^{13}C HSQC and COSY measurements the assignment of the ^{1}H signals were complete (see Table 2). The pK_a values were determined (the titration data and fitted curves are depicted on Figure 9). Based on previous work, (Mirzahosseini A. and Noszál B, 2016) we could calculate the group – specific standard redox potentials for the four cysteine residues. These redox potential values revealed that the thiol groups with the highest oxidation propensities will form disulfide linkage first, if the thiols are close enough to each other. CD measurements and molecular dynamics simulations verified the lack of any classical secondary structure of the peptide at pH 4.5 (for 3D structures see Figure 13).

As a result, we can state that the primary structure of the thiols and disulfides influences the physico – chemical properties, for instance the electron density around the sulfur atoms and the pK_a values, due to inductive effects. The reactivity of these molecules shows clearly different apparent and microscopic rate constants. Also, disulfide bonds tend to form first between cysteine residues of high protonation constants and low redox potentials.

6. Summary

In this study we examined the thiolate-disulfide reactions of MSH – CSSC and MSSM – CSH in order to gain insight into the GSH oxidation kinetics and the concomitant antioxidant properties. We determined pH-dependent apparent and pH-independent microscopic rate constants using quantitative ^{1}H-NMR and a new evaluation method. We observed that any group that increases the nucleophilicity of the thiolate or the electrophilicity of the disulfide linkage, raises the microscopic reaction rate constant and makes the thiol – disulfide reaction faster. Changing the pH has a bigger effect on the velocity of the reaction via apparent rate constant, increasing the relative abundance of the thiolate.

We also performed NMR measurements with the reduced derivative of α-conotoxin MI, a tetradecapeptide, and determined the group-specific pK_a values. In accordance with our previous hypothesis, the thiolate groups with the highest protonation constants and therefore highest oxidation propensities will form disulfide bonds first, unless a strong alternate conformational preference exists. We determined that the protonation state of the peptide greatly influences its conformation and indeed that thiolate groups with the highest pK_a values form disulfide bridge in the native form of the oxidized peptide.

7. References

Ai-Hua J, Muttenthaler M, Dutertre S, Himalaya SWA, Kaas Q, Craik DJ, Lewis RJ, Alewood PF. (2019) Conotoxins: Chemistry and Biology. Chem Rev, 119 (21): 11510-11549.

Akondi BK, Muttenthaler M, Dutertre S, Kaas Q, Craik DJ, Lewis RJ, Alewood PF. (2014) Discovery, synthesis and development of structure-activity relationships of conotoxins. Chem Rev, 114 (11): 5815-5847.

Azimi P, Ghiasvand R, Feizi A, Hariri M, Abbasi B. (2014) Effects of Cinnamon, Cardamom, Saffron and Ginger Consumption on Markers of Glycemic Control, Lipid Profile, Oxidative Stress and Inflammation in Type 2 Diabetes Patients. Rev Diabet Stud, 11 (3-4): 258-266.

Bucci E. (2009) Thermodynamic approach to oxygen delivery in vivo by natural and artificial oxygen carriers. Biophys Chem, 142: 1-6.

Butterfield DA, Boyd-Kimball D. (2018) Oxidative Stress, Amyloid-β Peptide and Altered Key Molecular Pathways in the Pathogenesis and Progression of Alzheimer's Disease. J Alzheimers Dis, 62: 1345-1367.

Carstens BB, Berecki G, Daniel JT, Lee HS, Jackson AVK, Tae H, Sadeghi M, Castro J, O'Donnell T, Deiteren A, Brierley SM, Craik DJ, Adams JD, Clark RJ. (2016) Structure-activity studies of cysteine-rich α-Conotoxins that inhibit high-voltage-activated calcium channels via $GABA_B$ receptor activation reveal a minimal functional motif. Angew Chem Int Ed Engl, 55 (15): 4692-4696.

Chatterjee M, Saluja R, Kanneganti S, Chinta S, Dikshit M. (2007) Biochemical and molecular evaluation of neutrophil NOS in spontaneously hypertensive rats. Cell Mol Biol, 53: 84-93.

Choi TG, Lee J, Ha J, Kim SS. (2011) Apoptosis signal-regulating kinase 1 is an intracellular inducer of p38 MAPK-mediated myogenic signalling in cardiac myoblasts. Biochim Biophys Acta, 1813: 1412-1421.

Crotty GF, Ascherio A, Schwarzschild MA. (2017) Targeting urate to reduce oxidative stress in Parkinson disease. Exp Neurol, 298: 210-224.

D’Amico E, Factor-Litvak P, Santella RM, Mitsumoto H. (2013) Clinical Perspective of Oxidative Stress in Sporadic ALS. Free Radic Biol Med, 65: 509-527.

Duque MH, Dias CS, Franco LO. (2019) Structural and functional Analyses of cone snail toxins. Mar Drugs, 17 (6): 370.

Faragó Z, Mirza A, Horváth D, Pálla T, Horváth P, Perczel A, Noszál B. (2021) Solution Structure and Acid-Base Properties of Reduced α-Conotoxin MI. Chem Biodivers, 18, e2100464

Gu F, Chauhan V, Chauhan A. (2015) Glutathione redox imbalance in brain disorders. Curr Opin Clin Nutr Metab Care, 18 (1): 89-95.

Gouda H, Yamazaki K, Hasegawa J, Kobayashi Y, Nishiuchi Y, Sakakibara S, Hirono S. (1997) Solution structure of α-Conotoxin MI determined by 1H-NMR spectroscopy and molecular dynamics simulation with the explicit solvent water. Biochim Biophys Acta, 1343: 327-334.

Gray WR, Rivier JE, Galyean R, Cruz LJ, Olivera BM. (1983) Conotoxin MI. disulfide bonding and conformational states. J Biol Chem, 258 (20): 12247-12251.

Hoffman SM, Nolin JD, McMillen DH, Wouters EFM, Janssen-Heininger YMW, Reynaert NL. (2015) Thiol redox chemistry: role of protein cysteine oxidation and altered redox homeostasis in allergic inflammation and asthma. J Cell Biochem, 116 (6): 884-892.

Leslie B. Poole. (2015) The Basics of Thiols and Cysteines in Redox Biology and Chemistry. Free Radic Biol Med, 0: 148-157.

Kastin AJ. Handbook of Biologically Active Peptides. Academic Press, Cambridge, 2013: 1721-1723.

Keire DA, Strauss E, Guo W, Noszál B, Rabenstein DL. (1992) Kinetics and equilibria of thiol/disulfide interchange reactions of selected biological thiols and related molecules with oxidized glutathione. J Org Chem, 57 (1): 123-127.

Klaunig JE, Wang Z. (2018) Oxidative stress in carcinogenesis. Curr Opin Toxicol, 7: 116-121.

Lebbe Eline KM, Tytgat J. (2016) In the picture: disulfide-poor conopeptides, a class of pharmacologically interesting compounds. J Venom Anim Toxins Incl Trop Dis, 22:30.

Mazák K, Noszál B. (2016) Advances in microspeciation of drugs and biomolecules: species-specific concentrations, acid-base properties and related parameters. J Pharm. Biomed. Anal. 130, 390-403,

Mirzahosseini A, Faragó Z, Noszál B. (2018) Determination of pH-independent rate constants of thiolate-disulfide redox transitions. New J Chem, 42: 11653-11659.
Mirzahosseini A, Noszál B. (2014) The species- and site-specific acid-base properties of biological thiols and their homodisulfides. J Pharm Biomed Anal, 95: 184-192.

Mirzahosseini A, Noszál B. (2016) Species-Specific Standard Redox Potential of Thiol-Disulfide Systems: A Key Parameter to Develop Agents against Oxidative Stress. Sci Rep, 6: 37596.

Mirzahosseini A, Somlyay M, Noszál B. (2015) Species-Specific Thiol-Disulfide Equilibrium Constant: A Tool To Characterize Redox Transitions of Biological Importance. J Phys Chem, 119 (32): 10191-10197.

Mossuto FM. (2013) Disulfide bonding in neurodegenerative misfolding diseases. Int J Cell Biol, 2013: 318319.

Nagy P. (2013) Kinetics and mechanisms of thiol-disulfide exchange covering direct substitution and thiol oxidation-mediated pathways. Antioxid Redox Signal, 18 (13): 1623-1641.

Szajewski RP, Whitesides GM. (1980) Rate Constants and Equilibrium Constants for Thiol-Disulfide Interchange Reactions Involving Oxidized Glutathione. J Am Chem Soc, 102 (6): 2011-2026.

Szakács Z, Noszál B. (1999) Protonation microequilibrium treatment of polybasic compounds with any possible symmetry. J Math Chem, 26: 139-155.

Tsetlin V, Utkin Y, Kasheverov I. (2009) Polypeptide and peptide toxins, magnifying lenses for binding sites in nicotinic acetylcholine receptors. Biochem Pharmacol, 78 (7): 720-731.

Valko M, Rhodes CJ, Monocol J, Izakovic M, Mazur M. (2006) Free radicals, metals and antioxidants in oxidative stress-induced cancer. Chem Biol Interact, 160: 1-40.

8. Bibliography of the candidate's publications

Faragó Z, Mirzahosseini A, Horváth D, Pálla T, Horváth P, Perczel A, Noszál B. (2021) Solution Structure and Acid-Base Properties of Reduced α-Conotoxin MI. Chem Biodivers, 18, e2100464

Mirzahosseini A, Faragó Z, Noszál B. (2018) Determination of pH-independent rate constants of thiolate-disulfide redox transitions. New J Chem, 42: 11653-11659.

9. Acknowledgments

I wish to acknowledge the support of FIKP (TKP) 2020 and the ÚNKP-20-4-I-SE-2, ÚNKP-20-4-II-SE-3, ÚNKP-17-4-I-SE-80 and ÚNKP-172-I-SE-17, New National Excellence Program of the Ministry for Innovation and Technology from the source of the National Research, Development and Innovation Fund. I wish to thank Dr. Balázs Balogh from the Department of Organic Chemistry, Semmelweis University and Dr. Dóra K Menyhárd from the Laboratory of Structural Chemistry and Biology, MTA-ELTE Protein Modelling Research Group, Institute of Chemistry, Eötvös Loránd University for their invaluable discussions and help in the molecular dynamics simulations.

I would like to thank my co-workers from the Department of Pharmaceutical Chemistry and above all, for Dr. Károly Mazák for his suggestions and my supervisors, Dr. Béla Noszál and Dr. Arash Mirzahosseini for their help and tireless support.